Journal Name

ARTICLE

Luminescence control in hybrid perovskites and applications

J. Albero and H. García

Received 00th January 20xx,
Accepted 00th January 20xx

DOI: 10.1039/x0xx00000x

www.rsc.org/

Hybrid metal halide perovskites have emerged as promissing semicondcutor materials for photovoltaic applications as consequence of their remarkable intrisic optoelectronic properties and their compositional flexibility. However, these properties have been also found suitable for applications in other different fields. Particularly, the photoluminescence properties of hybrid perovskite have demonstrated give rise to efficient light emitting devices as well as in lasing applications. In this manuscript we have reviewed the recent advances of hybrid perovskites in these fields paying attention to the perovskites composition design as a tool to modulate the luminescence properties in this kind of devices.

Introduction.

Inorganic and hybrid metal halide perovskites have attracted a considerable interest in the scientific community in the last years due to the high efficiency that can be reached on perovskite solar cells and other remarkable optoelectronic properties that they have demonstrated in different fields, beyond their use in solar cells. Indeed, metal halide perovskites present exceptional optic and electronic properties, that have determined that these materials are close to meet the commercial requirements for their use as semiconductor in photovoltaic applications, but being in addition easily solution-processed, and having affordable production costs. In particular, their high charge mobilities, long photoexcited carrier lifetime, relatively low band gap (~1.51 eV), small exciton binding energy (< 50 meV) and large light absorption coefficients in the visible and near-infrared (NIR) range of hybrid metal halide perovskites are among the reason behind their use in photovoltaics, obtaining increasing efficiencies from an initial value of 3.8% to overcome the 20% in a short period of time [1-3]. Despite the success of these materials in photovoltaic applications, their outstanding optoelectronic properties have given rise also to other applications in different fields such as sensing [4], photodetectors [5], light emitting devices (LED) [6], amplified spontaneous emission (ASE) and lasing [7]. Particularly for most of these uses, the exceptional photoluminescence quantum yields as well as long-lived emissions have especially attracted the attention, both in the development of LEDs, where internal quantum efficiencies exceeding 15% have already been reported in a wide range of tunable light emission spectra [8], as well as in optical gain and lasing [9]. In all these applications, photoluminescence plays a crucial role [10].

Instituto de Tecnología Química CSIC-UPV, Universitat Politècnica de València, Av. de los Naranjos s/n, 46022 Valencia, Spain
See DOI: 10.1039/x0xx00000x

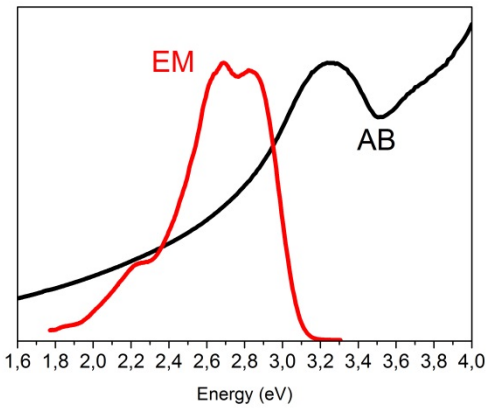

Figure 1. Normalized UV-Vis absorption (AB, black) and emission spectra (EM, red) of a mixed $CH_3NH_3PbCl_{x-1}(I_x)$ hybrid perovskite.

The luminescence is the photon emission in the UV-Vis-NIR region of radiation as a result of electronic excitation, either optical or electrical of a material. Hybrid metal halide perovskites have been found to exhibit an intense and broad band luminescence centered very near its absorption edge with a full width at half-maximum (fwhm) of approximately 100 meV (depending on the perovskite composition) at room temperature. The characteristic luminescence width has been generally found almost twice as broad as the spectral width of the absorption edge (i.e. 56 meV in $CH_3NH_3PbI_3$ hybrid perovskite). Moreover, photoluminescence maximum has been described slightly red shifted in energy (~30 meV), with respect to the band gap, this small shift being one of the main characteristics in their emission spectra. Figure 1 presents as example a normalized absorption and emission spectra for a mixed $CH_3NH_3PbCl_{x-1}(I_x)$ hybrid perovskite.

The mechanisms that govern the luminescence in hybrid perovskites have been widely studied, being confirmed that the emission spectra is independent of the excitation energy [11]. Therefore, the luminescence in these materials is homogeneous and fully broadened at every excitation

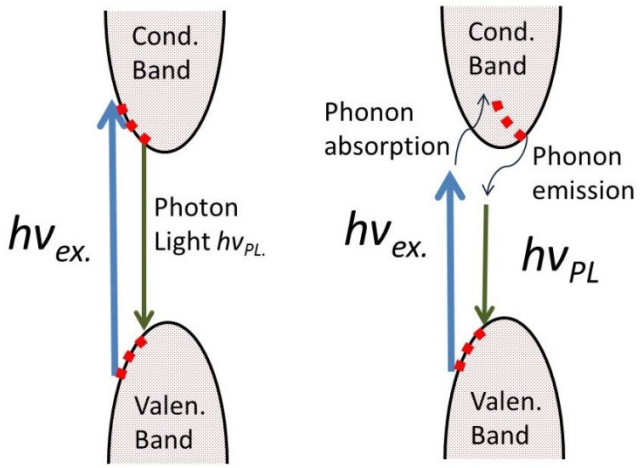

Scheme 1. Schematic band diagrams for photon emission (left) and phonon emission (right) processes, respectively.

wavelength. Different hypothesis have been proposed in order to explain the luminescent characteristics in hybrid metal halide perovskites. Among them the existence of additional intermediate states in the radiative recombination process with an extremely short lifetime (fs) has been proposed [11]. However, in these cases the emission broadening follows a Lorentzian distribution, while in the case of hybrid perovskites this distribution has been found Gaussian. Thus, it seems not probable that intermediate states could be responsible for the homogeneous and broad emission. Another possible explanation would be to attribute emission to polaronic effects, where photogenerated excitons strongly couples to the underlying lattice [11]. In this case, the luminescence would be significantly Stokes shifted from the absorption edge and, as commented before, the estimated Stokes-shift value in hybrid perovskites is small (around 30 meV). In addition, the high charge mobility and long diffusion length reported for these materials suggest that any polaronic effect would be negligible, although still possible. A third explanation, and the most widely accepted, has attributed to phonons present in the radiative recombination process as the cause of the broad-band emission. In this case the emission spectra would consist in the band-edge emission peak combined with a number of side bands due to phonons [11]. The changes in absorption edge and emission spectra at temperatures between 297 K and 77 K (specifically, evolution of two excitonic peaks was found at 160 K, where a transition from tetragonal to orthorhombic phase has been described) support this theory [11, 12], where the overall emission spectrum width decreases with temperature consistent with a smaller available phonon population. Scheme 1 illustrates the phonon emission mechanism.

Despite all this, the rational design of the hybrid perovskites composition has given rise to modulation of their luminescent properties [13]. This is not surprising since composition tuning and design have been widely exploited in photovoltaics in order to control spectral response, band alignment as well as other characteristics affecting the photovoltaic device performance [14]. In a similar way, accurate composition design of the hybrid perovskites is able to fine tune their luminescent quantum yield, emission spectrum and lifetime, among other properties, and therefore, besides the phenomenon of luminescence high control of the light-emitting device characteristics in lighting and lasing applications has been demonstrated. Even more, the compositional flexibility in the case of photo or electroluminescent devices has demonstrated to be wider than in the case of photovoltaics. This is due to the possibility to obtain suitable light emitting devices employing hybrid perovskites with 2D structures while in photovoltaic, the perovskite structure is restricted to 3D to achieve efficient light harvesting and improve charge transport issues [15]. Therefore, broader possibilities in composition are possible to alter light emission. In this manuscript we have reviewed the modulation of the main luminescent properties by the control of the compositional in hybrid metal halide perovskites as well as the implication that this large flexibility in luminescence control offers for the tuning of their optoelectronic properties with immediate application in the fields of light-emitting devices and lasing.

Luminescence properties control.

Hybrid organic-inorganic materials have attracted great interest in the last years due to the possibility of combining characteristic properties from both inorganic (high mobility, electrical pumping, band engineering) and organic materials (low cost processing technology, high room-temperature luminescence quantum yields, easy functionalization by derivatization), as well as generating new properties coming from the interactions between them. Hybrid metal halide perovskites are among the best examples of materials in which it is possible a large control of optoelectronic properties including tunable absorption and efficient light emission, among others, derived from the combination of atomic and molecular structures of the inorganic and organic counterparts. Although initially the large flexibility in the control of optoelectornic properties was attributed to the inorganic components, and in this initial understanding the organic parts have been simply considered convenient just for processability issues, it has been lately demonstrated that the organic parts can possess an active role determining also the optoelectronic properties of the hybrid material. As an example illustrating the active role of the organic component, Tang and co-workers fabricated a hybrid lead bromide perovskite containing as organic moiety an electroactive organic polymer. Di-substituted polyacetylene with long conjugated chains (Scheme 2) was intercalated into the inorganic framework producing an enhancement of the photoluminescence at 457 nm reaching 62% quantum yield that was much higher than that of the polymeric precursor without the inorganic counterpart [16].

In a different approach, Koshimizu and co-workers studied the effect in the photoluminescent properties of hybrid lead bromide perovskites with different organic moieties. $(C_4H_9NH_3)_2PbBr_4$, $(C_6H_5CH_2NH_3)_2PbBr_4$ and $(C_6H_5C_2H_4NH_3)_2PbBr_4$ 2D layered hybrid perovskites (see Figure 2) presented very different emission quantum efficiencies,

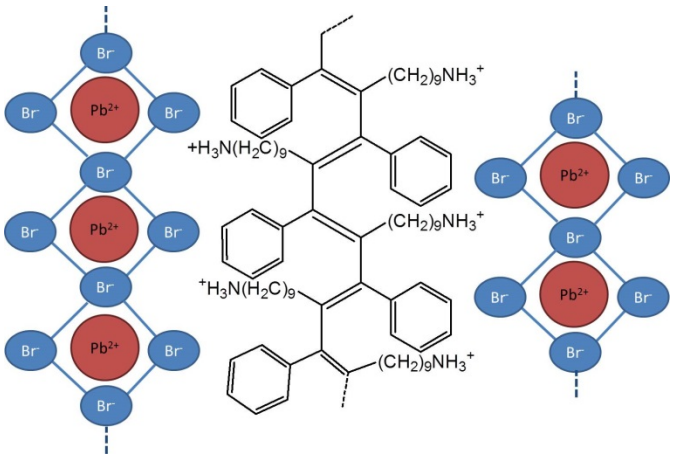

Scheme 2. Schematic illustration of di-substituted polyacetylene cation intercalated in the inorganic framework.

having the perovskite with phenyl groups ($(C_6H_5C_2H_4NH_3)_2PbBr_4$) the highest and the perovskite with C4 alkyl chains the lowest. The authors found that different organic molecules lead to different packing structure in the organic layer, which influences the structure in the inorganic layer as well. As consequence, the perovskite with the phenyl groups in the organic part produced structural distortion inside the $PbBr_6^{2-}$ octahedral with Br-Pb-Br bond angles of 171°, which contributed to decrease the Bohr exciton radius increasing the quantum efficiency and the emission decay rate, while with the other organic cations the Br-Pb-Br bond angle remained at 180° and lower quantum efficiencies and radiative decay rates were found [17]. The distortion of hybrid metal halide perovskites has been widely proposed as a tool for optical band gap tuning [18], and precise values of the optical band gaps have been predicted for hybrid perovskite materials by controlling the X-M-X (X: halide, M: metal) bond angles through accurate cation design [19] (Figure 2).

Papavassiliou et al. followed this argumentation and studied the photoluminescence of a set of 3D and 2D based $(SC)SnBr_3$, $(BC)_2SnBr_4$ and $(SC)(BC)_2SnBr_7$ hybrid perovskites, where SC

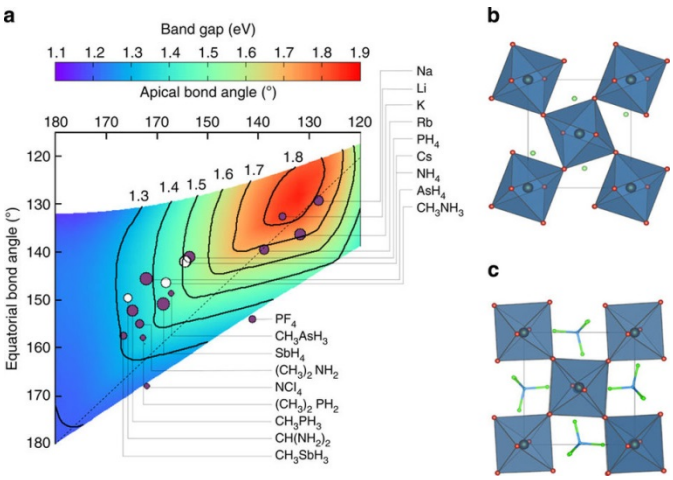

Figure 2. 2D map of the DFT band gap of the Platonic model of PbI_3-based perovskites as a function of metal-halide-metal bond angles (a) and atomistic models of (b) $LiPbI_3$ and (c) NCl_4PbI_3 metal halide perovskites exhibiting small and large metal-halide-metal bond angles, respectibely. With permission Ref. 19.

was $CH_3NH_3^+$ or Cs^+ and BC was $C_4H_9NH_3^+$, $CH_3C_6H_4CH_2NH_3^+$, $C_{12}H_{25}NH_3^+$, $C_{18}H_{37}NH_3^+$ or 1-naphthylmethyl ammonium group.

They found that, in general, materials with 2D structure showed stronger and broader bands than the 3D structure. Moreover, $(BC)_2SnBr_4$ compounds with short alkyl-chain lengths showed more intense and broader bands that the same compounds with long-alkyl chains. They attribute this behavior to the photoluminescence origin of the different compounds, which was proposed to arise from self-trapped excitons confined in the inorganic part for short-alkyl chain cations, while cation containing long-alkyl chains are proposed to exhibit free-excitonic states in the inorganic moieties [20].

On the other hand, colloidal formamidium lead halide pervoskites ($CH(NH_2)_2PbBr_3$) exhibiting a 3D structure have been reported demonstrating a high photoluminescence quantum efficiency of 55-65 % [21].

Apart from emission efficiency, bulky organic cations have been found very convenient to modulate other photoluminescence properties. For instance, Zhong et al. used C16 alkyl chain cation in the hybrid perovskite $(C_{16}H_{33}NH_3)_2PbI_4$ to induce reversible photoluminescence switch through induced perovskite aggregation. In this case, the long-alkyl chains promote good perovskite solubility in THF or acetone solvents, however, when H_2O or hexane were added the perovskite became less soluble, promoting self-aggregation of the material and precipitation. Interestingly, the perovskite solution was found nonemissive, and, in contrast, highly emissive when solvents inducing aggregation were added. The authors attribute this behavior to the formation of layered quantum-well structures when perovskite aggregates and dissolution of these 2D structures when high solubility solvents were used. The highly crystalline 2D quantum-well structures possess large dielectric mismatch and exhibit quantum confinement effects, these properties resulting in strong photoluminescence. On the contrary, dissolved perovskite exists as molecular entities that do not emit as consequence of their interaction with the surrounding solvent [22].

Other particular case where organic cations can play a key role in the photoluminescence properties of hybrid perovskites is the tuning of the emission spectrum. It is well accepted that, hybrid perovskites exhibits an intense and broad emission centered near its absorption edge. In fact, Boukheddaden and co-workers have reported broadband white-light emission at room temperatures coming from 2D $(C_6H_{11}NH_3)_2PbBr_4$ perovskites. They studied the origin of this white-light emission and they found that such emission is composed by two main bands, which were identify at low temperatures (< 90K). These emission peaks were attributed to free excitonic emission and shallow bound exciton, respectively. Although the contribution of these two bands to the overall emission varies with temperature and excitation energy, at room temperature the emission spectrum cover almost completely the visible spectrum (2.8-1.5 eV) [23]. On the contrary, when small cations were used in similar 3D lead bromide perovskites ($CH_3NH_3PbBr_3$ and $CH(NH_2)_2PbBr_3$) narrower emission spectra were obtained (2.38-2.14 eV) [24]. It is well established that the

organic cation in hybrid perovskites determines the perovskite-structure and dimensionality, and therefore its optoelectronic properties [14]. In 3D perovskite structure only small cations are allowed and size increase promotes structural distortion and as consequence a structural rearrangement from 3D to 2D or layered structures. As commented above, structural distortion in the inorganic net causes Bohr exciton radius as well as bandgap alteration, and therefore, changes in the photoluminescence characteristics.

It has to be remarked that the organic cation is not the only component determining the optoelectronic properties of hybrid metal halide perovskites and the inorganic counterparts also play a key role determining their photoluminescence properties [25]. For instance, the broadband white-light emission previously commented for $(C_6H_{11}NH_3)_2PbBr_4$ can be completely modified by halide substitution. Thus, $(C_6H_{11}NH_3)_2PbI_4$ perovskites have shown two strong green emission peaks at 2.44 and 2.31 eV, which have been attributed to free and localized excitons, respectively [26, 27]. Similarly, Kurunadasa et al. reported a (EDBE)PbX_4 perovskite family (EDBE = 2,2'-(ethylenedioxy)bis(ethylammonium); X = Cl, Br or I), where I^- anions produced sharp green emission centered at 515 nm with fwhm of 70 nm, while Br^- and Cl^- anions induced broad band white-light emission with maxima at 573 and 538 nm and fwhm of 215 and 208 nm for (EDBE)$PbBr_4$ and (EDBE)$PbCl_4$, respectively [28].

In a further extension of the use of halides to determine emission, the use of hybrid perovskites with mixed halides opens new possibilities for the fine tune of bandgap and optical properties. Thus, Ahmad et al. reported a systematic study of a series of $(C_{12}H_{25}NH_3)_2PbI_{4(1-y)}Br_{4y}$ ($0 < y < 1$) hybrid perovskites, reporting tunable photoluminescence as Br/I ratio function. These perovskites showed sharp and strong emissions, which variated from 510 to 350 nm as soon as the Br^- anions substituted I^- anions in the perovskite composition. The change in the photoluminescence was attributed to structural distortion of the inorganic crystal packing upon increase of the Br^- content in the Pb-I structure [25]. Atourki et al. also confirmed this observation in 3D $CH_3NH_3PbI_{3-x}Br_x$ ($x<1$) perovskites. They reported phase transformation from tetragonal to cubic when $0.6 > x > 0.4$. This gradual transformation induced bandgap tuning from 1.58 to 1.72 eV when the Br^- content increased in the perovskite structure, and therefore, the emission peaks ranged from 781 nm for pure $CH_3NH_3PbI_3$ up to 545 nm for pure $CH_3NH_3PbBr_3$ exhibiting intermediate emission maximum wavelengths for mixed I^-/Br^- compositions [29]. Similarly, Wang et al. found that Cl^- anions incorporation in the hybrid $CH_3NH_3PbBr_{3-x}Cl_x$ (x= 0.6-1.2) perovskite produced not only a change in emission peak wavelength and intensity, but also in the radiative recombination lifetime. Thus, increasing Cl^- amounts in the perovskite structure induced blue shift photoluminescence from 530 nm ($CH_3NH_3PbBr_3$) up to 484 nm ($CH_3NH_3PbBr_{1.8}Cl_{1.2}$). The emission efficiency was modified as well, obtaining a maximum intensity for $CH_3NH_3PbBr_{2.4}Cl_{0.6}$. Moreover, the introduction of such small amount of Cl^- in the structure was enough to produce an increase in the emission

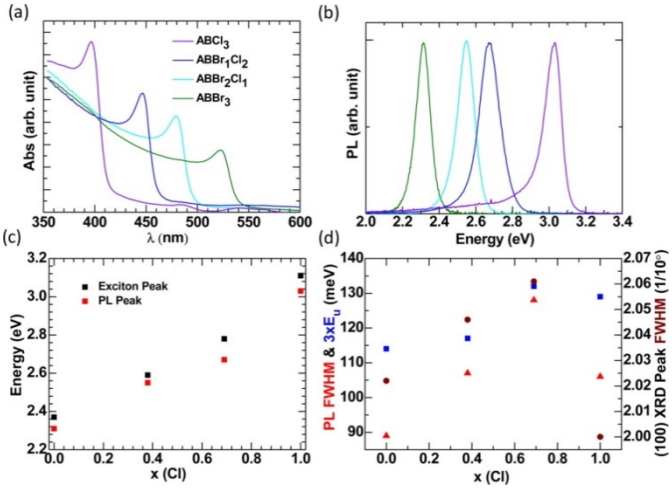

Figure 3. Absorption (a) and emission (b) spectra of $CH_3NH_3PbBr_{3-x}Cl_x$ (x = 0, 0.33, 0.66 and 1) perovskite. Excitonic peak and luminescence peak vs composition curve (c) and fwhm of the luminescence peak (d). With permission ref. 30

lifetime from 100 ns ($CH_3NH_3PbBr_3$) to 446 ns in the $CH_3NH_3PbBr_{2.4}Cl_{0.6}$ perovskite. Larger amounts of Cl^- in the composition caused reduced emission efficiencies and lifetimes. The authors suggested that the influence in the photoluminescence of small Cl^- percentages could be due to the high semiconducting quality of the mixed halide hybrid perovskites and low bulk defect density induced by the presence of small amounts of Cl^- in the perovskite composition [13]. Nonetheless, theoretical calculations have revealed that the optoelectronic properties in $CH_3NH_3PbBr_{3-x}Cl_x$ perovskites are governed by Pb 6p and halide p orbitals. While conduction band edge is totally due to Pb 6p orbitals and is not sensitive to compositional changes, the valence band maximum edge is originated by hybridization of bonding and antibonding states of halogens p orbitals and Pb 6s orbitals. Thus, upon Cl^- introduction in $CH_3NH_3PbBr_{3-x}Cl_x$ perovskites, the valence band edge configuration changes from Br 4p states, when $0<x<0.33$, combination of Br 4p and Cl 3p in $0.33<x<0.66$, and Cl 3p in $x> 0.66$. As consequence, incorporation of Cl^- ions replace Br 4p states by Cl 3p in the uppermost valence band, shifting the valence band edge for $x \geq 0.33$, and therefore, increasing the band gap. Other consequence of the band gap increase is its influence in the excitons coulomb field. Since optical properties are dominated by excitonic effects, increase in Cl^- concentration produces larger exciton binding energy due to the decrease in the dielectric constant [30] (Figure 3).

Besides the compositional effects in the optoelectronic properties of hybrid metal halide perovskites, there are other important parameters that can be altered during the perovskite preparation and can allow a better control of photoluminescence properties in the final material. Particle size of the hybrid perovskite crystals is one of them, particularly when measuring photoluminescence of thin films. Yan and coworkers have demonstrated photoluminescence intensity enhancement in hybrid metal halide perovskite not only changing the halogen composition, but also by varying the concentration of the precursors during the perovskite synthesis. That is, they found that the photoluminescence

efficiency depends on the $CH_3NH_3Br/PbBr_2/PbCl_2$ ration in the synthesis. Thus, the photoluminescence intensity of the $CH_3NH_3PbBr_{3-x}Cl_x$ perovskite was enhanced only when high CH_3NH_3Br concentration was used due to the formation of smaller crystals than at low concentrations. It has been widely accepted that small crystals size produce more dense and uniform films than large crystals, which lead to voids and non-uniform films. Besides, a proper election of the Br^-/Cl^- molar ratio was found to inhibit the formation of clusters, obtaining optimum emission intensity when $CH_3NH_3Br/PnBr_2/PbCl_2$ molar ratio was set to 2:0.8:0.2 [31]. In a very similar way, highly luminescent $CH_3NH_3PbBr_3$ nanoparticles with 83% quantum yield have been prepared by fine-tuning the molar ratio between CH_3NH_3Br, $PbBr_2$ and octylammonium bromide as capping ligand [32].

Petrozza and co-workers have studied the relationship between crystallite dimensions and photoluminescence properties, and they found that changing the average crystal size from nm to µm the optical band gap and photoluminescence lifetime could be tuned. Thus, larger crystals (> 1 µm) rendered smaller band gap (1.61 eV) and long lifetimes (100 ns). In contrast, smaller crystals (< 250 nm) presented larger band gaps (1.63 eV) and emission lifetime of about 2 ns. The authors proposed that this behavior could be attributed to higher radiative recombination in small crystals rather than in larger ones [33]. In a different study, photoluminescence peak tuning was achieved by annealing temperature control of $CH_3NH_3PbBr_{3-x}Cl_x$ perovskites. An increase in the annealing temperature resulted in a red shifted emission peak. In this case, the authors suggest that chlorine removal at increasing temperatures is responsible for to the change in emission peak, since pure $CH_3NH_3PbBr_3$ perovskites have reported smaller bandgap [34]. Alternatively, Rogach et al. described a ligand-assisted synthetic method to precipitate $CH_3NH_3PbBr_3$ perovskite quantum dots with fine control on the average particle size and narrow distribution through the fine tune of precipitation temperature. Due to quantum confinement effect, the precise control of the particle size produced bandgap tuning, obtaining $CH_3NH_3PbBr_3$ perovskite quantum dots of 1.8, 2.8 and 3.6 nm at precipitation temperatures of 0, 30 and 60 ^oC, respectively. The size dependent band gap resulted in photoluminescence peaks located at 2.61, 2.48 and 2.38 eV, respectively [35].

The compositional flexibility of metal halide perovskites has been found as one of their main characteristic to tune both optical and electronic properties. Therefore, besides the rational cation design and engineered halide composition, many different metal cations can be employed in the perovskite structure. The combination of the already commented compositional and synthetic strategies with different metals open new ways to achieve interesting photoluminescence properties. For instance, Zhang et al. prepared a layered hybrid $NH_3(CH_2)_5NH_3MnCl_4$ pervoskite, narrow orange emission band centered at 581 nm (fwhm = 60 nm). While Mn^{2+} in octahedral an tetrahedral coordination exhibit red and green emissions, respectively, this 2D perovskite shows this characteristic emission, which has been attributed to the distortion of the $MnCl_4$ octahedra [36].

It must be commented that although the present review is focused on luminescence properties control of hybrid organic-inorganic perovskites, the reported strategies to modulate optoelectronic properties in hybrid perovskites can be applied also in the inorganic perovskites. For instance, Kovalenko and co-workers reported the preparation of inorganic $CsPbX_3$ perovskites, where the compositional modulation of the halogen anion with Cl^-, Br^- or I^- and their mixtures Cl^-/Br^- and Br^-/I^- provide tunable emission peak in the entire visible spectral region (from 410 to 700 nm) with really narrow fwhm (12- 42 nm), outstanding emission quantum yields from 50 to 90% and photoluminescence lifetimes in the range between 1 to 29 ns. In addition, postsynthetic treatments based on ion-exchange reactions is a general methodology to compositional fine-tuning of all these photoluminescence properties [37, 38]. Similarly, Pan et al. described the synthesis of $CsPbX_3$ nanoparticles (X = Cl, Br or I) with highly tunable photoluminescence peaks ranging from 440 to 682 nm by using different fatty acids as capping ligands. They found that shorter capping agents like butyric acid provided red-shifted emission peaks rather than the longer fatty acids as oleic acid for each halogen in the composition, thus obtaining a wide range of emission colors [39]. In different approach, Alivisatos et al. reported a temperature controlled synthesis of highly luminescence (quantum yield ~ 84%) colloidal $CsPbBr_3$ peroskites, providing green emitting nanocubes (150 ^oC), cyan emitting nanoplates with 20 nm lateral size (130 ^oC) and blue emission nanoplates with 200-300 nm lamellar structures (90 ^oC). Figure 4 shows TEM images of $CsPbBr_3$ crystallites obtained at different temperatures of the synthesis and photographs of their characteristic emission [40]. Similarly, Manna and co-workers prepared blue emitting $CsPbBr_3$ nanoplatelets, green emitting $CsPbBr_3$ nanocubes, orange emitting $CsPbI_3$ nanosheets and red emitting $CsPbI_3$ nanocubes. They found that the combination of $CsPbBr_3$ nanoplatelets and $CsPbBr_3$ and $CsPbI_3$ nanocubes, among other possible combinations, exhibited apparent white-light emission upon UV excitation due to the overlapping of their individual emission of each component [41].

As previously commented for hybrid metal halide perovskites, the metal in all inorganic perovskites can be exchanged in order to search interesting photoluminescence properties of

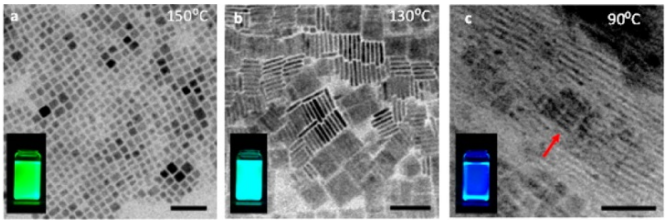

Figure 4. Influence of the reaction temperature with the $CsPbBr_3$ perovskite morphology and luminescence properties. (a) At 150 ^0C, green emitting 8-10 nm nanocubes, (b) at 130 ^0C, cyan emitting nanoplates with 20 nm lateral dimention and (c) at 90 ^0C blue emitting thin nanoplatelets (scale bar 50 nm in all pictures). With permission ref. 40.

inorganic perovskites. In this way, $CsSnX_3$ (X = Cl, $Cl_{0.5}Br_{0.5}$, Br, $Br_{0.5}I_{0.5}$, I) perovskites nanocrystals were synthetized and the tunable photoluminescence from the visible to the NIR part of the spectrum was investigated. They found that Sn-containing perovskite presented red-shifted bandgaps when compared with Pb-containing perovskites due to the higher electronegativity of Sn cation. Compositional changes in halide anions of Sn perovskite produce band gap tuning from 480 to 940 nm approximately. In addition, temperature control during the synthesis of $CsSnBr_3$ nanocrystals between 125 and 170 ^{o}C provided optical band gap tuning from 1.97 to 1.82 eV [42].

Recently, a completely different approach based on doping of perovskites has been reported and the photoluminescence properties of Yb^{2+}-doped $CsCaX_2$ and $CsSrX_3$ (X = Cl,Br or I) perovskites have been investigated. All the Yb^{2+}-doped perovskites presented intense blue-violet emissions, where the violet emissions were assigned to spin-forbidden transitions, while the blue emission was correlated as spin-allowed transition in the Yb^{2+} ions. Moreover, upconversion photoluminescence from Yb^{3+}/Mn^{2+} ABF_3 (A = K^+, Rb^+ and Cs^+; B = Mg $^{2+}$, Zn^{2+} and Cd^{2+}) perovskites has been demonstrated upon 976 nm laser excitation observing emission in the visible region. The co-doped Yb^{3+}/Mn^{2+} perovskites exhibited intense single photoluminescence band between 550 and 610 nm depending on the inorganic cation and the metal in the perovskite composition. This singular emission arises from coupled Yb^{3+}-Mn^{2+} transitions with very long emission lifetime decays (25-45 ms) arises [43, 44].

In summary, similarly to hybrid organic-inorganic perovskites also inorganic metal halide perovskites have demonstrated a plethora of promising photoluminescence properties which can be controlled through adequate composition design, synthetic procedures and post-synthetic treatments, annealing conditions, capping ligands and even ions doping.

Luminescence control in perovskite-based light emitting diodes (PeLEDs).

Metal halide perovskites have demonstrated unique optical and electronic properties, besides low cost production, easy processing, high charge-carrier mobility and mechanical and thermal stability. For that reason, these materials have attracted in the last years a considerable interest in optoelectronics, especially in their application as light harvester layers in photovoltaic devices. Alternatively, their striking luminescence properties have opened a new range of possible applications. The use of metal halide perovskites in electroluminescent devices is due to their strong photoluminescence, color purity, tunable emission spectrum and their compatibility with organic semiconductors [45]. These characteristics promoted their investigation as emissive layers in light emitting devices some decades ago [46-48]. However, electroluminescence from these materials could only be achieved efficiently at very low temperatures due to thermal ionization and delocalization issues at room temperature. The small exciton binding energy reported in these materials, which highly benefits charge separation in photovoltaic devices due to the easy exciton splitting into free charges, was found a problem in electroluminescence devices that require e^-/h^+ recombination, making their applicability at room

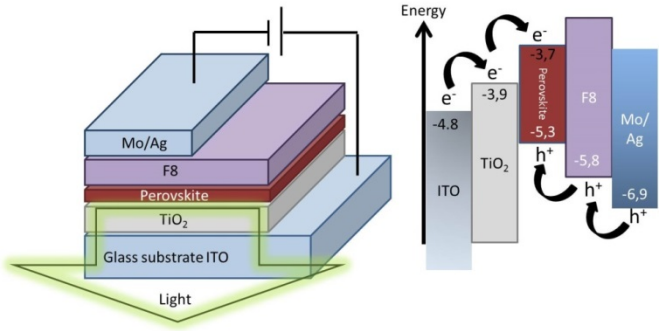

Scheme 3. PeLED architecture (left) and energy level diagram respect vacuum containing electron and hole blocking layers.

temperature challenging. Nevertheless, in 2014, Friend et al. designed a PeLED where the perovskite was placed between charges and enhance the electroluminescence at room two large-bandgap semiconductors in order to confine the temperature [6] (see Scheme 3). Moreover, the emitting perovskite layer was designed particularly thin in order to spatially confine electrons and holes in a small region. Thus perovskite layer between electron and hole blocking films (TiO_2 as hole blocking and as electron blocking poly (9,9-dioctylfluorene) (F8) see structure in Scheme 4). Charge confinement was achieved by sandwiching nanometric perovskite layer, thus, enhancing emission through the radiative e^-/h^+ recombination (Scheme 3). This breakthrough gave rise to the firsts PeLEDs based on hybrid perovskites, with configurations ITO/TiO_2/$CH_3NH_3PbI_{3-x}Cl_x$/F8/Mo-Ag (red emission) and ITO/PEDOT:PSS/$CH_3NH_3PbBr_3$/F8/Mo-Ag (green emission), working at room temperature. The green PeLEDs demonstrated a luminance of 364 cd/m^2 at 123 mA/cm^2, exhibiting 0.1 % external quantum efficiency [6]. Although these devices still presented modest efficiencies, the flexibility in the composition and emission properties of perovskites makes these materials a good candidates as emissive layers in light

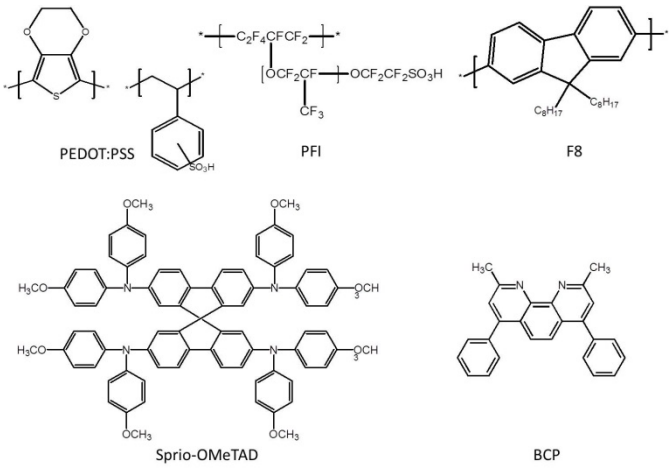

Scheme 4. Molecular structures of PEDOT:PSS, PFI, F8, Spiro-OMeTAD and BCP.

emitting diodes and a new research line started up in order to optimize their luminescence in devices.

In this sense, Mora-Sero et al reported NIR electroluminescence (emission peak at 773 nm) from $CH_3NH_3PbI_{3-x}Cl_x$ based PeLED. In this case, the PeLED was configured with TiO_2 as hole blocking and electron injection layer and the organic molecule spiro-OMeTAD (see Scheme 4) as electron blocking and hole injection layer, rendering a radiance of 7.1 W/sr·m^2 at 232 mA/cm^2 and an external quantum efficiency (EQE) of 0.48% [49].

Subsequently, Kabra et al. explored the emission shift from green to blue with $CH_3NH_3Pb(Br_{3-x}Cl_x)_3$ perovskite. In this case, the PeLED was built using PEDOT:PSS as hole injector and the derivative fullerene PCBM as electron injector. Green electroluminescence was obtained from $CH_3NH_3PbBr_{1.86}Cl_{1.14}$ anion mixtures, obtaining modest 1.2 cd/m^2 and 1.7 cd/m^2 blue emission from $CH_3NH_3PbBr_{1.06}Cl_{1.92}$ anions mix [50].

Not surprisingly in view of the previously commented changes in the emission anion exchange has been widely used in order to tune the electroluminescence in PeLEDS of hybrid perovskites. For instance, Yang et al. employed this method in order to convert $CH_3NH_3PbBr_3$ perovskite nanorod array into $CH_3NH_3PbI_3$ without alteration of the crystal morphology. In both cases PeLEDS were prepared using PEDOT:PSS as hole and (F8) as electron injection layers. The emission was successfully shifted from 533 nm using pure Br^- perovskite up to 782 nm when Br^- was exchanged by I^- [51]. On the contrary, when colloidal nanocrystal metal halide perovskite mixtures were used in order to cover the complete visible spectrum, its compositional instability was observed and unwanted spectral shift due to spontaneous anion exchange [52]. For instance, Snaith et al. prepared $CH_3NH_3PbX_3$ (X=Cl^-, Br^-, I^-) nanocrystal perovskites and subsequently mixed them in different ratios achieved white light emission among other interesting color mixtures (Figure 5). However, simply mix of different nanocrystals containing different halides in the composition promote spontaneous anion exchange and emission shift in thin films. In order to avoid this undesirable anion exchange, they blended the different nanocrystal solution with a transparent and insulating polystyrene polymer prior to film deposition. In this way a stable device, without emission shift white light PeLEDs was obtained [53]. In similar approach, Rui et al. integrated different $CsPbX_3$ (X= Br^-, I^-) nanocrystal perovskites in mesoporous silica matrix in order to enhance thermal and photochemicalstability and avoid ion exchange. They applied this composite successfully in white-ligth inorganic PeLED for backlight displays [54]. Stability issues have been also observed in single composition metal halide perovskite films in PeLEDs. In these cases, the instability origin has been found when fluorene derivatives as F8 are used [55]. Instead, the use of metal oxides as hole blocking and electron injection layers has been found a convenient alternative. In a similar way to previously discussed PeLEDs using TiO_2 as electron injection, ZnO and Mg- layers have been deposited instead of F8 by Credgington et al. [56] In this study, $CH_3NH_3PbBr_3$ perovskite PeLEDs were prepared and the effect of F8 and $Zn_{1-x}Mg_xO$ electron injector layers compared. It has been found that the substitution of the organic layer by metal oxides could enhance the luminance and lower turn-on voltage as well as improve air stability [56, 57].

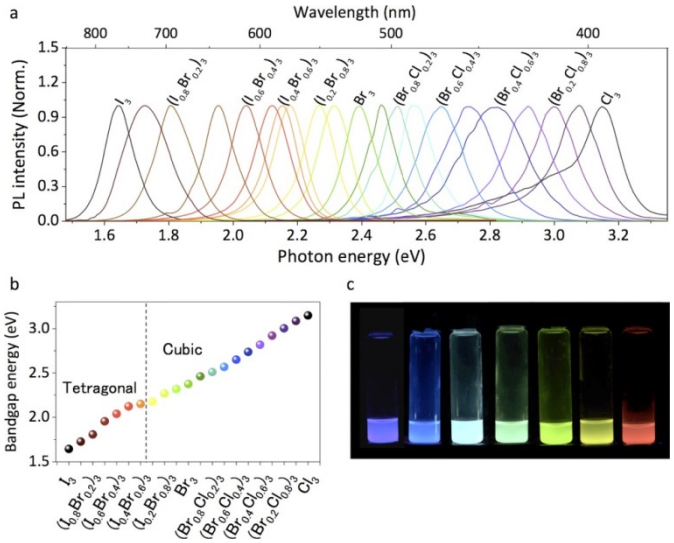

Figure 5. Emission spectra (a), band gap (b) and photograph of emission from (0.3 OA:0.7 MA)PBX_3 (MA= $CH_3NH_3^+$) (X=I^-,Br^-, Cl^-). With permission ref. 53.

Nevertheless, injection layers are not the only source of leakages and instability in PeLEDs. The poor coverage of metal halide perovskite films has been found to be the main limiting factor to achieve efficient PeLEDs [58]. Pinholes and defects in the perovskite films creates electrical shunt pathways, which promotes that injected charges pass from one electrode to the other without recombine radiatively in the emitter layer, leading to losses in electroluminescence yield. Different methods have been investigated in order to improve perovskite film coverage, and thus, reduce current leakage losses. Greenham et al. developed a method where perovskite and a polyimide precursor (PIP) dielectric were blended in solution and deposited in order to form thin film composites. The PIP formed a polymeric matrix where perovskites still conserved electrical contact between them and the injection layers, although without the presence of pinholes, reducing the current losses and achieving an external quantum efficiency of 1.2 %. PeLEDs containing F8 and PEDOT:PSS as electron and hole injection layers, respectively, were built with $CH_3NH_3PbBr_3$ perovskite embedded in PIP, obtaining a luminance of 200 cd/m^2 at 3.1 mA/cm^2 while in the absence of PIP a current of 580 mA/cm^2 was needed to achieve similar luminance [59]. Rogarch et al. introduced a perfluorinated ionomer (PFI) film in between the hole injection layer (PEDOT:PSS) and the perovskite emissive layer ($CsPbBr_3$). The PeLED current density with the PFI layer was lowered from 826 to 688 mA/cm^2 at 7 V, obtaining a maximum luminance of 1377 cd/m^2 and 340 cd/m^2 with and without PFI, respectively [60].

Perovskite film formation has gained considerable importance in order to reach the target of preparing uniform and smooth films. In this sense, Song et al. introduced HBr into the perovskite precursor in order to increase the solubility of the inorganic components in the perovskite. This higher solubility resulted in the formation of continuous and uniform perovskite films leading to full-coverage films and efficient

PeLEDs. Optimized $CH_3NH_3PbBr_3$ PeLEDS containing 6 v/v % HBr in the DMF/HBr cosolvent have shown 3490 cd/m^2 at 4.3 V, exhibiting a luminance efficiency of 0.43 cd/A and 0.1% EQE [61]. Similar approach to improve the morphology of perovskite particles was adopted by Wu et al. [58] In this case a solvent/non-solvent N,N-dimethylformamide/chlorobenzene (DMF/CB) mixture was used to improve the $CH_3NH_3PbBr_3$ film morphology. Optimized PeLEDs using 10:4 v:v DMF/CB mixed solvents produced films with dense morphology exhibiting 3868 cd/m^2 and EQE of 0.13% with current efficiency of 0.54 cd/A.

A completely different approach was investigated by Yu et al. [62] who blended $CH_3NH_3PbBr_3$ perovskite with poly(ethylene oxide) (PEO) in order to obtain a homogeneous thin film composite. On the contrary to the previously discussed PIP/perovskite blend, where PIP is a dielectric polymer, PEO not only improves the film coverage, but also its conductivity since PEO has been reported to possess good properties as ionic conductor [62]. Optimized devices prepared by printing deposition techniques on both rigid ITO/glass and flexible CNTs/polymer substrates in air conditions have shown a maximum of 21014 cd/m^2 luminance with EQE of 1.1% [63].

Interfacial treatments in nanocrystal perovskite-based thin films have been used as well to control the morphology of the perovskite films and increase the PeLEDs efficiency. Gao and co-workers synthetized colloidal $CH_3NH_3PbBr_3$ nano platelets using octylammonium bromide as long-chain capping ligand and they used these to prepare PeLEDs using PEDOT:PSS as hole injection and bathocuproine (BCP,see structure in Scheme 4) as electron injection layers. The as-prepared PeLEDs exhibited 10590 cd/m^2, such a remarkable brightness was achieved when poly(9-vinylcarbazole):2-(4-biphenylyl)-5-phenyl-1,3,4-oxadiazole (PVK:PBD) was deposited between the BCP and the colloidal perovskite layers. Control devices without the PVK:PBD layer showed a luminance of 1113 cd/m^2 as well as high current leakage probably due to the presence of pinholes formed in the nanoplatelets perovskite layer. The introduction of the bipolar PVK:PBD was found key for optimizing the film morphology, improving the interfacial quality of the perovskite layer by removing the pinholes and reducing the surface roughness from 45.3 to 34 .6 nm. Moreover, the charge transport and current losses were improved when PVK:PBD polymer layer was added due to the reduction of pinholes in the emitting layer [64].

Generally defects and crystal imperfections exhibit a strong influence on the photoluminescence properties of materials. In the case of hybrid perovskites, Xiong et al. reported the synthesis of amorphous $CH_3NH_3PbBr_3$ nanoparticles and preparation of PeLEDs exhibiting 3.8% EQE and 11.49 cd/A current efficiency. The origin of this impressive efficiency using amorphous hybrid perovskite nanoparticles was proposed to be the nearly negligible photoluminescence dependence with the temperature that exhibited by nanocrystals. This observation is indicating that nonradiative recombination pathways do not occur in a significant degree in amorphous perovskite nanocrystals, and therefore, the photoluminescence quantum yield in amorphous nanocrystals has been found higher than in polycrystalline films. In addition, the widely reported weak exciton binding energy (<50 meV) in bulk hybrid perovskites is, on the one hand, improving the performance of photovoltaic devices due to the easy charge separation into free charges at room temperature, however, on the other hand, decreasing the luminous efficiency in PeLEDs, as commented before. In contrast, nanocrystals have been found to confine excitons more efficiently than bulk materials and therefore, the smaller the nanoparticle the higher the exciton binding energy. In summary, the superior exciton confinement in colloidal perovskite nanoparticles and the negligible non-radiative recombination observed in the amorphous nanoparticles are responsible for the PeLEDs high performance employing amorphous colloidal perovskite nanoparticles [65]. Similar approach was used by Lee and co-workers, who prepared $CH_3NH_3PbBr_3$ nanocrystals (99.7 nm in average) in order to confine the excitons, limiting their diffusion length to 67 nm. Besides, an excess of CH_3NH_3Br amount in the synthesis mixture avoided the formation of Pb metal atoms in the final perovskite sample, which are well known to quench excitons, reducing device efficiency. This modifications produced current efficiency of 42.9 cd/A and 8.53% EQE, which is the highest performance described so far [66].

W. Huand et al. have recently reported PeLEDs exhibiting 11.7% EQE. This high efficiency was achieved through a very convenient combination of 2D and 3D structures which gave rise to self-organized multiple quantum wells. The authors attributed this high device efficiency to the confinement of injected charges in the quantum wells. The electrons and holes are rapidly accumulated in the quantum wells, where remain confined until recombination with elevated efficiency [67]. Moreover, remarkable good stability was achieved with the multiple quantum wells structure, obtaining a drop of half of the initial EQE after 2h of continuous applied bias.

As it is being commented hybrid organic-inorganic perovskites share with all inorganic metal halide perovskites many common traits. Thus, no surprisingly inorganic metal halide perovskite have also achieved good efficiencies in PeLEDS. In a recent report, dual phase $CsPbBr_3$-$CsPbBr_5$ perovskite was used as emissive layer in PeLEDs, exhibiting a maximum luminance of 3853 cd/m^2, with a current efficiency of 8.98 cd/A and 2.21% EQE. In this case, the secondary phase $CsPbBr_5$ in the cubic $CsPbBr_3$ structure was proposed to reduce the exciton diffusion length as well as to dismish the density of trapping sites, confining the charges in the emissive layer and enhancing the current efficiency [68].

As an overall summary of the evolution of the field, the combination of a fine composition tuning and engineered synthetic methods has boosted metal halide perovskites based light-emitting devices efficiency up to promising values in a short period of time. Although the maximum external quantum efficiency is still lower than reported values (~20 %) for organic light emitting diodes (OLEDs) [69], the compositional flexibility and the ability to from homogeneous thin films, acquired from the photovoltaic field in most cases, makes reasonable to anticipate that in few years these materials will

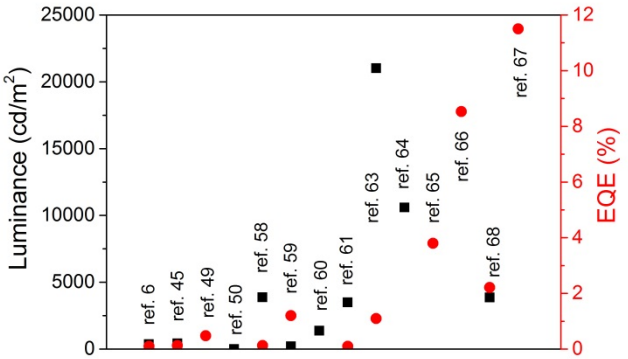

Figure 6. Reported luminance and external quantum efficiency for selected PeLEDs with different compositions and synthetic protocols.

overpass the device efficiency needed for considering commercial applications. This progress in device efficiency is summarized in Figure 6.

Light amplification by stimulated emission of radiation in perovskites.

As it has been commented in previous sections hybrid metal halide perovskites have demonstrated outstanding photoluminescence properties which can be precisely engineered through composition and particle size and morphology control. The bright and highly efficient photoluminescence of these materials have allowed the preparation of efficient light emitting devices with a large variety of colors, including white light emission. Similarly, other optoelectronic applications derived from their striking photoluminescence properties have been investigated recently. Inspired by their high efficient photoluminescence, Sum and collaborators reported in 2014 solution processed hybrid metal halide perovskites with promising optical gain [7]. The authors realized that photoluminescence intensity of a cavity-free $CH_3NH_3PbI_3$ thin film increased linearly with the excitation energy at relatively low pumping levels, but at a certain threshold (12 ± 2 μJ/cm^2) the emission intensity increased exponentially. In addition, the typical broadband emission was collapsed after a certain threshold pump level, evolving to a sharp peak at 788 nm (see Figure 7). These finding make $CH_3NH_3PbX_3$ (X=Cl, Br, I) to qualify as suitable materials for stable amplified spontaneous emission (AES) at relatively low thresholds, exhibiting spectral tunability in the visible region (390 – 790 nm) depending on the halide composition [7]. The authors studied the ASE behavior of $CH_3NH_3PbI_3$ and compared with some of the most promising nanocrystal quantum dots and organic materials in this field. They found that ZnSe and CdS nanocrystals or solution-processed organic thin films (i.e. poly[9,9-dioctylfluorene-co-9,9-di(4-methoxyphenyl)-fluorene]) presented threshold carrier densities one magnitude order larger than $CH_3NH_3PbI_3$ (aprox. 1.7 x 10^{18} cm^{-3}).

They attributed the lower charge carrier density threshold in $CH_3NH_3PbI_3$ to the ultralow defect densities and slow Auger recombination that these perovskites have demonstrated, while in organic materials intrinsic losses derived from

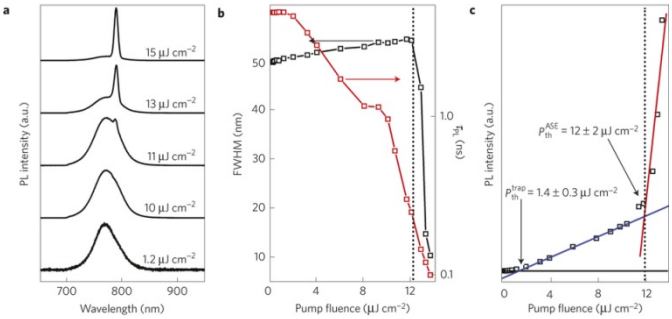

Figure 7. (a) Photoluminescence spectra from a $CH_3NH_3PbI_3$ film excited at 600 nm, 150 fs and 1 kHz laser pulses with increasing pump fluence. (b) fwhm of the emission peak and average transient luminescence lifetime as a function of the pump fluence. (c) Photoluminescence as a function of pump fluence. With permission of ref. 7

intermolecular recombination is a general unavoidable phenomenon and the nanocrystal quantum dots have demonstrated important losses due to Auger recombination and limited charge transport. Therefore, hybrid metal halide perovskites have been proposed as potential materials for practical laser devices [7].

The mechanism of the ASE in these materials has been investigated. It has been proposed that in the absence of cavities in the solution processed perovskite thin films the optical amplification for lasing could be generated as consequence of the random scattering. This random scattering could originate from the polycrystalline grain boundary in a material having particles of different sizes and phases that co-exists and are randomly distributed in the film [70]. In agreement with this proposal, the specific crystal size and shape have been found crucial for perovskite laser generation and, therefore, different methodologies for perovskite crystal morphology control have been developed. In a recent report, Zhao et al. described the use of surfactants to form micelles as soft templates in the synthesis of microstructured $CH_3NH_3PbBr_3$ perovskites films [71]. Through this method the crystal growth was modulated by the different surfactants and the controlled formation of specific perovskite microcrystals achieved. Indeed, 1D microwires and 2D square microplates were fabricated using octadecylammonium bromide and dodecylammonium bromide surfactants, respectively, and efficient radiative emission at very low threshold obtained. Moreover, the proposed lasing mechanism was confirmed, since the 1D microwires presented strong lasing from the wire ends when the pump energy achieved 112 μJ/cm^2 and in the 2D microplates the lasing occurs on the four edges of the square microplate, as can be observed in Figure 8, when the pump exceed a 62 μJ/cm^2 threshold [71]. For that reason, perovskite microplates and nanowires have been commonly prepared and ultralow laser thresholds and unidirectional lasing emissions obtained [72-74].

The main drawback for commercial application of microplates and microwires of hybrid perovskites is the account of multiple

lasing modes due to their relatively large size distribution, and therefore, the "polychromatic" lasing emission observed in these materials [75]. Song and collaborators reported a method to induce monochromatic laser operation consisting in arranging the emitting microplates around the lasing microplate actually emitting. This method consisted in selecting a smaller $CH_3NH_3PbBr_3$ microplate (around 16 x 14 μm), which upon femtosecond laser pump above 28 μ J/cm^2

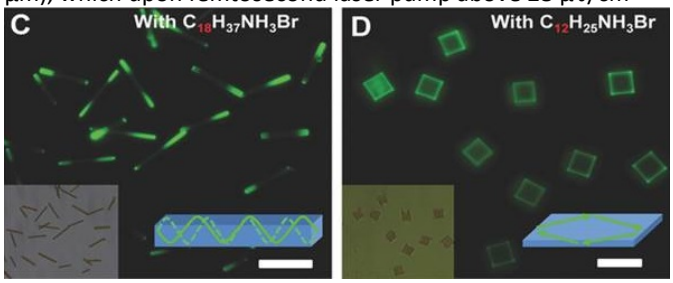

Figure 8. Photolumincescence and bright-field (left insets) images of 1 D microwires and 2 D microplates in $CH_3NH_3PbBr_3$ perovskites films. Scale bars 10 μm. With permission of ref. 71.

from lasers of different wavelength between 5 and 15 nm around 553 nm, and put in contact with a second bigger microplate (around 21 x 16 μm) by micromanipulation shows laser emission. This second microplate was not pumped to ensure all lasing modes come from the smaller microplate. It was observed that by this spatial arrangement the smaller microplate was the only one emitting with one reduced the number of lasing wavelengths [75].

On the other hand, improved perovskite films morphology and crystallinity have been found very convenient in order to achieve high performance ASE devices [33, 76]. In this regard, Hou et al. designed a sequential deposition process by using binary solvent mixtures of DMF and DMSO in order to control the morphology and crystallinity of hybrid metal halide perovskites ($CH_3NH_3PbI_3$) thin films. Upon solvent ratio optimization, smooth (8.49 ± 0.99 nm) and highly crystalline films were obtained, improving the ASE threshold at 54.1 μJ/cm^2 and decreasing the ASE full width at half maximum (fwhm) up to 8.16 nm [76]. Following a similar approach, Nurmikko and co-workers developed a preparation method for subwavelength surface roughness in pinhole-free and densely packed solution-processed perovskite ($CH_3NH_3PBI_3$) thin films [77]. In this method, the authors used a host solvent to spin cast a solution with the perovskite precursors, and subsequent injection of an extraction solvent during spinning induced the formation pinhole-free perovskite films as it was previously reported [78]. However, in this case the authors took advantage of the stronger Pb-O bond and coordination ability of DMSO rather than DMF with lead iodide to use it as host solvent. Therefore, the no uniform grain sizes distributed across the films, usually obtained when DMF is used as host solvent, were significantly improved with DMSO as consequence of the retarded crystallization process upon controlled toluene dripping. In this protocol a uniform distribution of the perovskite nucleates is observed [77]. Moreover, this procedure allowed the deposition of the perovskite film on a 2D photonic crystal resonator. By adjusting the periodicity and radius of the nanopatterned substrates and depositing continuous and conformal perovskite films on top of the 2D photonic crystals, low threshold, single wavelength, spatially coherent laser operation in the NIR was achieved [77]. Other methods have been successfully applied in order to grown perovskites on spherical structures. For instance, atomic layer deposition has been used to coat silica microspheres, and stable optical gain from the perovskite film was observed from 75 μj/cm^2 threshold for 24 h [79].

Different strategies have been carried out to further enhance the optically pumped ASE in hybrid metal halide perovskites. Thus, Snaith and co-workers sandwiched a $CH_3NH_3PbI_3$ perovskite thin film within a cavity composed by a cholesteric liquid crystal and a metal back reflector. They found that the threshold for ASE from the sandwiched perovskite was two magnitude orders lower than the measured in cavity-free perovskite films [80]. And more recently, the same authors have reported the use of a well-known periodical structure (the "*distributed feedback cavity*")[81] in which optical reflections are provided by Bragg scattering from an interference grating and the active medium. In this case, $CH_3NH_3PbI_{3-x}Cl_x$ perovskite was evaporated on top of a nanoimprinted polymer resist to form hybrid perovskites-based *distributed feedback cavities*. It was found that varying the grating periodicity emission between 770 and 793 nm could be obtained [82]. In addition, lower fwhm and excitation thresholds (0.32 – 2.11 μJ/cm^2) have been obtained than those reported for other lasing structures with similar perovskite materials (10 – 20 μJ/cm^2) [7, 82, 83].

The substitution of the organic cation, the metal or the halide anion and their combinations has demonstrated to be a major advantage to tune the optical and physical properties of these hybrid materials in photovoltaic and light emitting devices. The remarkably lasing performance at low thresholds that hybrid metal halide perovskites have demonstrated can be also improved through the compositional flexibility that these materials can allow. In this sense, despite the good results reported in $CH_3NH_3PbX_3$ (X = I, Cl, Br), these materials have shown poor thermal stability due to the reversible phase transition between tetragonal and cubic at 57 ^{0}C and chemical instability upon air exposure [84, 85]. For that reason, Jin and co-worker studied perovskites stability in lasing applications when methyl ammonium (MA) cation was totally or partially replaced by formamidium (FA) [86], which have been previously reported to lead to lower bandgap and improved thermal and moisture stability [87]. They found tunable lasing behavior in the visible and NIR at low thresholds. In addition, improved photostability at room temperature was demonstrated using $FAPbI_3$ and MABr-stabilized $FAPBI_3$ perovskites under aproximatelly 10^8 shots of sustained illumination at 402 nm pulsed laser excitation, which was found one order higher than the $MAPBI_3$ laser operation [86].

On the other hand, all-inorganic metal halide perovskites have been also reported to exhibit notable ASE. In this regard, Kovalenko et al. reported low-threshold ASE (less than 5 μJ/cm^{-2}) from ~10 nm monodisperse $CsPbX_3$ (X = Cl, Br or I, or mixed Cl/Br and Br/I) nanocrystals [88]. The observed ASE was obtained in the entire visible spectra (440 – 700 nm)

depending on the halogen composition. Moreover, different lasing modes from $CsPbX_3$ nanocrystals were obtained both coating silica microspheres and forming thin films. Furthermore, passivated $CsPbBr_3$ nanocrystals have been reported to show improved photostability under continuous pump excitation under ambient conditions for at least 34 h [89]. This passivation was carried out by an ionic pair composed by didodecyl dimethylammonium sulfide ($S^{2-}DDA^{+}$). The capping ligand produced a clear improvement of the nanocrystal photoluminescence quantum yield from 49% to 70%, while the emission peak remained unaltered [89].

Conclusions

The present review has shown the remarkable photoluminescence properties of hybrid metal halide perovskites and how these properties in terms of emission wavelength, quantum yield and lifetimes can be varied by changes in the composition and in the morphology and size of the particles. In this way, all the wavelength range from the visible to the NIR can be accessed by using the appropriate perovskite sample. Combination of different hybrid perovskites can even lead to white light emission. The most likely photoluminescence mechanism seems to be phono-coupled charge carrier recombination. It has been shown in the review that the flexibility in the design of perovskites for applications based on photoluminescence is much larger than for their use in photovoltaic devices and that in the case of photoluminescence 2D layered and 1D wired structures are also very interesting due to their optimal performance. Throughout the review it has been illustrated that hybrid metal halide perovskites are a subclass of inorganic metal halide perovskites and that all the properties of these materials can probably be also developed in the hybrid perovskites. The review has described application of photoluminescence in the preparation of light emitting devices and also in amplified spontaneous emission. The field of hybrid perovskite light emitting devices has benefited considerably of the advances and understanding of film formation that has been intensely investigated for application in photovoltaic devices and remarkable efficiencies has been already achieved.

Considering that hybrid organic metal halide perovskites are currently under much investigation, it can be easily predicted that the field will grow in the near future and that further improvements in the efficiency of electroluminescence devices and amplified spontaneous emission will be reached by further control of the composition, crystal structure and particle morphology as well as additives, bringing these materials close to applications. However, less attention has been paid to device stability in PeLEDs and perovskite based lasers in comparison with photovoltaic devices. Further research will be carried out in the near future in this regard, where compositional engineering will play a key role.

Acknowledgements

Financial support by the Spanish Ministry of Economy and Competitiveness (Severo Ochoa, and CTQ2015-69563-CO2-R1) and by the Generalitat Valenciana (Prometeo 2013-014) is gratefully acknowledged. J.A. also thanks the Universitat Politécnica de Valéncia for a postdoctoral scholarship.

Notes and references

1. A. Kojima, K. Teshima, Y. Shirai and T. Miyasaka, *Journal of the American Chemical Society*, 2009, **131**, 6050-6051.
2. H. Zhou, Q. Chen, G. Li, S. Luo, T.-b. Song, H.-S. Duan, Z. Hong, J. You, Y. Liu and Y. Yang, *Science*, 2014, **345**, 542-546.
3. N. J. Jeon, J. H. Noh, W. S. Yang, Y. C. Kim, S. Ryu, J. Seo and S. I. Seok, *Nature*, 2015, **517**, 476-480.
4. C. Muthu, S. R. Nagamma and V. C. Nair, *RSC Advances*, 2014, **4**, 55908-55911.
5. Y. Fang, Q. Dong, Y. Shao, Y. Yuan and J. Huang, *Nat Photon*, 2015, **9**, 679-686.
6. Z.-K. Tan, R. S. Moghaddam, M. L. Lai, P. Docampo, R. Higler, F. Deschler, M. Price, A. Sadhanala, L. M. Pazos, D. Credgington, F. Hanusch, T. Bein, H. J. Snaith and R. H. Friend, *Nat Nano*, 2014, **9**, 687-692.
7. G. Xing, N. Mathews, S. S. Lim, N. Yantara, X. Liu, D. Sabba, M. Grätzel, S. Mhaisalkar and T. C. Sum, *Nat Mater*, 2014, **13**, 476-480.
8. P. Docampo and T. Bein, *Accounts of Chemical Research*, 2016, **49**, 339-346.
9. D. Yang, C. Xie, J. Sun, H. Zhu, X. Xu, P. You, S. P. Lau, F. Yan and S. F. Yu, *Advanced Optical Materials*, 2016, **4**, 1053-1059.
10. S. Colella, M. Mazzeo, A. Rizzo, G. Gigli and A. Listorti, *The Journal of Physical Chemistry Letters*, 2016.
11. C. Wehrenfennig, M. Liu, H. J. Snaith, M. B. Johnston and L. M. Herz, *The Journal of Physical Chemistry Letters*, 2014, **5**, 1300-1306.
12. K. Wu, A. Bera, C. Ma, Y. Du, Y. Yang, L. Li and T. Wu, *Physical Chemistry Chemical Physics*, 2014, **16**, 22476-22481.
13. M. Zhang, H. Yu, M. Lyu, Q. Wang, J.-H. Yun and L. Wang, *Chemical Communications*, 2014, **50**, 11727-11730.
14. J. Albero, A. M. Asiri and H. Garcia, *Journal of Materials Chemistry A*, 2016, **4**, 4353-4364.
15. L. N. Quan, M. Yuan, R. Comin, O. Voznyy, E. M. Beauregard, S. Hoogland, A. Buin, A. R. Kirmani, K. Zhao, A. Amassian, D. H. Kim and E. H. Sargent, *Journal of the American Chemical Society*, 2016, **138**, 2649-2655.
16. H. Xu, J. Sun, A. Qin, J. Hua, Z. Li, Y. Dong, H. Xu, W. Yuan, Y. Ma, M. Wang and B. Z. Tang, *The Journal of Physical Chemistry B*, 2006, **110**, 21701-21709.
17. N. Kawano, M. Koshimizu, Y. Sun, N. Yahaba, Y. Fujimoto, T. Yanagida and K. Asai, *The Journal of Physical Chemistry C*, 2014, **118**, 9101-9106.
18. A. Amat, E. Mosconi, E. Ronca, C. Quarti, P. Umari, M. K. Nazeeruddin, M. Grätzel and F. De Angelis, *Nano Letters*, 2014, **14**, 3608-3616.
19. M. R. Filip, G. E. Eperon, H. J. Snaith and F. Giustino, *Nat Commun*, 2014, **5**, 5757.
20. G. C. Papavassiliou, M.-S. Vidali, G. Pagona, G. A. Mousdis, N. Karousis and I. Koutselas, *Journal of Physics and Chemistry of Solids*, 2015, **79**, 1-6.

21. A. Perumal, S. Shendre, M. Li, Y. K. E. Tay, V. K. Sharma, S. Chen, Z. Wei, Q. Liu, Y. Gao, P. J. S. Buenconsejo, S. T. Tan, C. L. Gan, Q. Xiong, T. C. Sum and H. V. Demir, *Scientific Reports*, 2016, **6**, 36733.
22. Y. Niu, F. Zhang, Z. Bai, Y. Dong, J. Yang, R. Liu, B. Zou, J. Li and H. Zhong, *Advanced Optical Materials*, 2015, **3**, 112-119.
23. A. Yangui, D. Garrot, J. S. Lauret, A. Lusson, G. Bouchez, E. Deleporte, S. Pillet, E. E. Bendeif, M. Castro, S. Triki, Y. Abid and K. Boukheddaden, *The Journal of Physical Chemistry C*, 2015, **119**, 23638-23647.
24. J. Dai, H. Zheng, C. Zhu, J. Lu and C. Xu, *Journal of Materials Chemistry C*, 2016, **4**, 4408-4413.
25. S. Ahmad, J. J. Baumberg and G. Vijaya Prakash, *Journal of Applied Physics*, 2013, **114**, 233511.
26. K. Gauthron, J. S. Lauret, L. Doyennette, G. Lanty, A. Al Choueiry, S. J. Zhang, A. Brehier, L. Largeau, O. Mauguin, J. Bloch and E. Deleporte, *Opt. Express*, 2010, **18**, 5912-5919.
27. A. Yangui, S. Pillet, A. Mlayah, A. Lusson, G. Bouchez, S. Triki, Y. Abid and K. Boukheddaden, *The Journal of Chemical Physics*, 2015, **143**, 224201.
28. E. R. Dohner, A. Jaffe, L. R. Bradshaw and H. I. Karunadasa, *Journal of the American Chemical Society*, 2014, **136**, 13154-13157.
29. L. Atourki, E. Vega, B. Marí, M. Mollar, H. Ait Ahsaine, K. Bouabid and A. Ihlal, *Applied Surface Science*, 2016, **371**, 112-117.
30. N. K. Kumawat, M. N. Tripathi, U. Waghmare and D. Kabra, *The Journal of Physical Chemistry A*, 2016, **120**, 3917-3923.
31. J. Yan, B. Zhang, Y. Chen, A. Zhang and X. Ke, *ACS Applied Materials & Interfaces*, 2016, **8**, 12756-12763.
32. S. Gonzalez-Carrero, R. E. Galian and J. Perez-Prieto, *Journal of Materials Chemistry A*, 2015, **3**, 9187-9193.
33. V. D'Innocenzo, A. R. Srimath Kandada, M. De Bastiani, M. Gandini and A. Petrozza, *Journal of the American Chemical Society*, 2014, **136**, 17730-17733.
34. M. Wei, Y.-H. Chung, Y. Xiao and Z. Chen, *Organic Electronics*, 2015, **26**, 260-264.
35. H. Huang, A. S. Susha, S. V. Kershaw, T. F. Hung and A. L. Rogach, *Advanced Science*, 2015, **2**, 1500194.
36. X.-H. Lv, W.-Q. Liao, P.-F. Li, Z.-X. Wang, C.-Y. Mao and Y. Zhang, *Journal of Materials Chemistry C*, 2016, **4**, 1881-1885.
37. L. Protesescu, S. Yakunin, M. I. Bodnarchuk, F. Krieg, R. Caputo, C. H. Hendon, R. X. Yang, A. Walsh and M. V. Kovalenko, *Nano Letters*, 2015, **15**, 3692-3696.
38. G. Nedelcu, L. Protesescu, S. Yakunin, M. I. Bodnarchuk, M. J. Grotevent and M. V. Kovalenko, *Nano Letters*, 2015, **15**, 5635-5640.
39. S. Wei, Y. Yang, X. Kang, L. Wang, L. Huang and D. Pan, *Chemical Communications*, 2016, **52**, 7265-7268.
40. Y. Bekenstein, B. A. Koscher, S. W. Eaton, P. Yang and A. P. Alivisatos, *Journal of the American Chemical Society*, 2015, **137**, 16008-16011.
41. F. Palazon, F. Di Stasio, Q. A. Akkerman, R. Krahne, M. Prato and L. Manna, *Chemistry of Materials*, 2016, **28**, 2902-2906.
42. T. C. Jellicoe, J. M. Richter, H. F. J. Glass, M. Tabachnyk, R. Brady, S. E. Dutton, A. Rao, R. H. Friend, D. Credgington, N. C. Greenham and M. L. Böhm, *Journal of the American Chemical Society*, 2016, **138**, 2941-2944.
43. M. Suta, W. Urland, C. Daul and C. Wickleder, *Physical Chemistry Chemical Physics*, 2016, **18**, 13196-13208.
44. E. Song, Z. Chen, M. Wu, S. Ding, S. Ye, S. Zhou and Q. Zhang, *Advanced Optical Materials*, 2016, **4**, 788-808.
45. Y.-H. Kim, H. Cho, J. H. Heo, T.-S. Kim, N. Myoung, C.-L. Lee, S. H. Im and T.-W. Lee, *Advanced Materials*, 2015, **27**, 1248-1254.
46. M. Era, S. Morimoto, T. Tsutsui and S. Saito, *Applied Physics Letters*, 1994, **65**, 676-678.
47. T. Hattori, T. Taira, M. Era, T. Tsutsui and S. Saito, *Chemical Physics Letters*, 1996, **254**, 103-108.
48. K. Chondroudis and D. B. Mitzi, *Chemistry of Materials*, 1999, **11**, 3028-3030.
49. O. A. Jaramillo-Quintero, R. S. Sanchez, M. Rincon and I. Mora-Sero, *The Journal of Physical Chemistry Letters*, 2015, **6**, 1883-1890.
50. N. K. Kumawat, A. Dey, A. Kumar, S. P. Gopinathan, K. L. Narasimhan and D. Kabra, *ACS Applied Materials & Interfaces*, 2015, **7**, 13119-13124.
51. A. B. Wong, M. Lai, S. W. Eaton, Y. Yu, E. Lin, L. Dou, A. Fu and P. Yang, *Nano Letters*, 2015, **15**, 5519-5524.
52. E. T. Hoke, D. J. Slotcavage, E. R. Dohner, A. R. Bowring, H. I. Karunadasa and M. D. McGehee, *Chemical Science*, 2015, **6**, 613-617.
53. S. Pathak, N. Sakai, F. Wisnivesky Rocca Rivarola, S. D. Stranks, J. Liu, G. E. Eperon, C. Ducati, K. Wojciechowski, J. T. Griffiths, A. A. Haghighirad, A. Pellaroque, R. H. Friend and H. J. Snaith, *Chemistry of Materials*, 2015, **27**, 8066-8075.
54. H.-C. Wang, S.-Y. Lin, A.-C. Tang, B. P. Singh, H.-C. Tong, C.-Y. Chen, Y.-C. Lee, T.-L. Tsai and R.-S. Liu, *Angewandte Chemie International Edition*, 2016, n/a-n/a.
55. L. Romaner, A. Pogantsch, P. Scandiucci de Freitas, U. Scherf, M. Gaal, E. Zojer and E. J. W. List, *Advanced Functional Materials*, 2003, **13**, 597-601.
56. R. L. Z. Hoye, M. R. Chua, K. P. Musselman, G. Li, M.-L. Lai, Z.-K. Tan, N. C. Greenham, J. L. MacManus-Driscoll, R. H. Friend and D. Credgington, *Advanced Materials*, 2015, **27**, 1414-1419.
57. Z.-F. Shi, X.-G. Sun, D. Wu, T.-T. Xu, S.-W. Zhuang, Y.-T. Tian, X.-J. Li and G.-T. Du, *Nanoscale*, 2016, **8**, 10035-10042.
58. B. Jiao, X. Zhu, W. Wu, H. Dong, B. Xia, J. Xi, T. Lei, X. Hou and Z. Wu, *Nanoscale*, 2016, **8**, 11084-11090.
59. G. Li, Z.-K. Tan, D. Di, M. L. Lai, L. Jiang, J. H.-W. Lim, R. H. Friend and N. C. Greenham, *Nano Letters*, 2015, **15**, 2640-2644.
60. X. Zhang, H. Lin, H. Huang, C. Reckmeier, Y. Zhang, W. C. H. Choy and A. L. Rogach, *Nano Letters*, 2016, **16**, 1415-1420.
61. J. C. Yu, D. B. Kim, E. D. Jung, B. R. Lee and M. H. Song, *Nanoscale*, 2016, **8**, 7036-7042.
62. J. Li, S. G. R. Bade, X. Shan and Z. Yu, *Advanced Materials*, 2015, **27**, 5196-5202.
63. S. G. R. Bade, J. Li, X. Shan, Y. Ling, Y. Tian, T. Dilbeck, T. Besara, T. Geske, H. Gao, B. Ma, K. Hanson, T. Siegrist, C. Xu and Z. Yu, *ACS Nano*, 2016, **10**, 1795-1801.
64. Y. Ling, Z. Yuan, Y. Tian, X. Wang, J. C. Wang, Y. Xin, K. Hanson, B. Ma and H. Gao, *Advanced Materials*, 2016, **28**, 305-311.

65. J. Xing, F. Yan, Y. Zhao, S. Chen, H. Yu, Q. Zhang, R. Zeng, H. V. Demir, X. Sun, A. Huan and Q. Xiong, *ACS Nano*, 2016, **10**, 6623-6630.
66. H. Cho, S.-H. Jeong, M.-H. Park, Y.-H. Kim, C. Wolf, C.-L. Lee, J. H. Heo, A. Sadhanala, N. Myoung, S. Yoo, S. H. Im, R. H. Friend and T.-W. Lee, *Science*, 2015, **350**, 1222-1225.
67. N. Wang, L. Cheng, R. Ge, S. Zhang, Y. Miao, W. Zou, C. Yi, Y. Sun, Y. Cao, R. Yang, Y. Wei, Q. Guo, Y. Ke, M. Yu, Y. Jin, Y. Liu, Q. Ding, D. Di, L. Yang, G. Xing, H. Tian, C. Jin, F. Gao, R. H. Friend, J. Wang and W. Huang, *Nat Photon*, 2016, **10**, 699-704.
68. X. Zhang, B. Xu, J. Zhang, Y. Gao, Y. Zheng, K. Wang and X. W. Sun, *Advanced Functional Materials*, 2016, **26**, 4595-4600.
69. B. S. Kim, K. S. Yook and J. Y. Lee, *Scientific Reports*, 2014, **4**, 6019.
70. T. S. Kao, Y.-H. Chou, C.-H. Chou, F.-C. Chen and T.-C. Lu, *Applied Physics Letters*, 2014, **105**, 231108.
71. W. Zhang, L. Peng, J. Liu, A. Tang, J.-S. Hu, J. Yao and Y. S. Zhao, *Advanced Materials*, 2016, **28**, 4040-4046.
72. H. Zhu, Y. Fu, F. Meng, X. Wu, Z. Gong, Q. Ding, M. V. Gustafsson, M. T. Trinh, S. Jin and X. Y. Zhu, *Nat Mater*, 2015, **14**, 636-642.
73. Q. Liao, K. Hu, H. Zhang, X. Wang, J. Yao and H. Fu, *Advanced Materials*, 2015, **27**, 3405-3410.
74. K. Wang, W. Sun, J. Li, Z. Gu, S. Xiao and Q. Song, *ACS Photonics*, 2016, **3**, 1125-1130.
75. S. Liu, W. Sun, Z. Gu, K. Wang, N. Zhang, S. Xiao and Q. Song, *RSC Advances*, 2016, **6**, 50553-50558.
76. L. Qin, L. Lv, Y. Ning, C. Li, Q. Lu, L. Zhu, Y. Hu, Z. Lou, F. Teng and Y. Hou, *RSC Advances*, 2015, **5**, 103674-103679.
77. S. Chen, K. Roh, J. Lee, W. K. Chong, Y. Lu, N. Mathews, T. C. Sum and A. Nurmikko, *ACS Nano*, 2016, **10**, 3959-3967.
78. N. J. Jeon, J. H. Noh, Y. C. Kim, W. S. Yang, S. Ryu and S. I. Seok, *Nat Mater*, 2014, **13**, 897-903.
79. B. R. Sutherland, S. Hoogland, M. M. Adachi, C. T. O. Wong and E. H. Sargent, *ACS Nano*, 2014, **8**, 10947-10952.
80. S. D. Stranks, S. M. Wood, K. Wojciechowski, F. Deschler, M. Saliba, H. Khandelwal, J. B. Patel, S. J. Elston, L. M. Herz, M. B. Johnston, A. P. H. J. Schenning, M. G. Debije, M. K. Riede, S. M. Morris and H. J. Snaith, *Nano Letters*, 2015, **15**, 4935-4941.
81. H. Kogelnik and C. V. Shank, *Applied Physics Letters*, 1971, **18**, 152-154.
82. M. Saliba, S. M. Wood, J. B. Patel, P. K. Nayak, J. Huang, J. A. Alexander-Webber, B. Wenger, S. D. Stranks, M. T. Hörantner, J. T.-W. Wang, R. J. Nicholas, L. M. Herz, M. B. Johnston, S. M. Morris, H. J. Snaith and M. K. Riede, *Advanced Materials*, 2016, **28**, 923-929.
83. F. Deschler, M. Price, S. Pathak, L. E. Klintberg, D.-D. Jarausch, R. Higler, S. Hüttner, T. Leijtens, S. D. Stranks, H. J. Snaith, M. Atatüre, R. T. Phillips and R. H. Friend, *The Journal of Physical Chemistry Letters*, 2014, **5**, 1421-1426.
84. G. Niu, X. Guo and L. Wang, *Journal of Materials Chemistry A*, 2015, **3**, 8970-8980.
85. T. A. Berhe, W.-N. Su, C.-H. Chen, C.-J. Pan, J.-H. Cheng, H.-M. Chen, M.-C. Tsai, L.-Y. Chen, A. A. Dubale and B.-J. Hwang, *Energy & Environmental Science*, 2016, **9**, 323-356.
86. Y. Fu, H. Zhu, A. W. Schrader, D. Liang, Q. Ding, P. Joshi, L. Hwang, X. Y. Zhu and S. Jin, *Nano Letters*, 2016, **16**, 1000-1008.
87. G. E. Eperon, S. D. Stranks, C. Menelaou, M. B. Johnston, L. M. Herz and H. J. Snaith, *Energy & Environmental Science*, 2014, **7**, 982-988.
88. S. Yakunin, L. Protesescu, F. Krieg, M. I. Bodnarchuk, G. Nedelcu, M. Humer, G. De Luca, M. Fiebig, W. Heiss and M. V. Kovalenko, *Nat Commun*, 2015, **6**.
89. J. Pan, S. P. Sarmah, B. Murali, I. Dursun, W. Peng, M. R. Parida, J. Liu, L. Sinatra, N. Alyami, C. Zhao, E. Alarousu, T. K. Ng, B. S. Ooi, O. M. Bakr and O. F. Mohammed, *The Journal of Physical Chemistry Letters*, 2015, **6**, 5027-5033.

1